Supporting Information for "Variability in Records of Phanerozoic Seawater Sulfate," by T. M. Present, J. F. Adkins, and W. W. Fischer (2020).

Age assignment and data compilation

Histograms of the four compiled proxy datasets are shown in Supporting Figure S1, and summary statistics are reported in Supporting Table S1. Supporting Table S2 includes each data source and a description of the age model applied to the reference, with applicable citations. Supporting File *d34S_Data.xlsx* tabulates the compiled $\delta^{34}S$ data with the proxy material, assigned age, and data source.

Variography

Semivariance is the variance—per point—of the difference between equally spaced pairs of measurements (Webster & Oliver, 2007, p. 54). Variograms are functions relating semivariance to the distance between the points, called the lag. In this paper, the lag is the age difference between two samples. The empirical variogram describing the semivariance of the $\delta^{34}S$ data, γ, as a function of lag, h, is estimated for $N(h)$ pairs of data with that lag:

$$\gamma(h) = \frac{1}{2}\frac{1}{N(h)}\sum_{i=1}^{N(h)}[\delta^{34}S(t_i) - \delta^{34}S(t_i + h)]^2$$

Although the variance of pairs of data may change as a function of t, the semivariance does not. If the variance was not a function of t, then the semivariance would simply mirror the covariance (Webster & Oliver, 2007, p. 55).

Formulating variance as the square of the difference is sensitive to outliers in the data. By decreasing the order of the variogram estimator from 2 and applying a correction to maintain a normal distribution, a variogram that unweights tails on the distribution and thus is more robust to outliers is developed (Cressie & Hawkins, 1980). A variogram order of 0.5 was used here:

$$\gamma_{robust}(h) = \frac{1}{2}\frac{\left[\frac{1}{N(h)}\sum_{i=1}^{N(h)}\sqrt{|\delta^{34}S(t_i) - \delta^{34}S(t_i + h)|}\right]^4}{0.457 + \frac{0.494}{N(h)} + \frac{0.045}{N^2(h)}}$$

Empirical variograms for detrended $\delta^{34}S$ data from each proxy in each era are shown in Supporting Figure S2. Because timeseries are temporally autocorrelated, the semivariance at short lags is less than at long lags. Additionally, the maximum variability over the domain of interest is described by the population variance, and the semivariance approaches this value over an interval called the range. The population variance is often referred to as the "sill" in geospatial analysis.

At the shortest lags, the semivariance is not zero. This uncorrelated variance represents the variability of $\delta^{34}S$ measurements unresolved by sampling. It is often referred to as the "nugget" in geospatial analysis.

The approach of semivariance to the population variance can be described with a model of the structure of the empirical variogram. For our 2-dimensional (time and $\delta^{34}S$) data, covariance can be modelled by the overlap of two circles populated randomly following a Poisson distribution (Webster & Oliver, 2007, p. 87). This circular variogram model describes semivariance as a function of lag, h, given the range, a, sill, c, and nugget, n:

$$\gamma_{model}(h) = \begin{cases} n + c\left\{1 - \frac{2}{\pi}\cos^{-1}\left(\frac{h}{a}\right) + \frac{2h}{\pi a}\sqrt{1 - \frac{h^2}{a^2}}\right\} & \text{for } h \leq a, \\ n + c & \text{for } h > a \end{cases}$$

To fit the variogram model to the empirical variogram, we diagnosed the nugget and sill from the data and visually adjusted the range: the nugget is the empirical semivariance computed at the mean minimum time between all pairs of data, and the sill is the population variance. We only require the model to estimate uncertainty in the $\delta^{34}S$ records—we are not attempting to predict $\delta^{34}S$ compositions in rocks that haven't been sampled. Therefore, it was unnecessary to employ more agnostic strategies to select a variogram model and fit it to the empirical variogram.

Kriging

Kriging is both a method of interpolating the data and for modelling the uncertainty around the unobserved, interpolated point (Gebbers, 2010). The expected value of an interpolated point is simply a weighted average of the data. The weights are calculated using the variogram model that describes semivariance as a function of distance from observations such that the estimated semivariance of the unobserved point (called the kriging variance) is minimized.

Detrending the data is necessary to ensure that the mean is constant (first-order stationary), but results in improper estimation of total variance by failing to account for both uncertainty and bias in the detrending (Lark & Webster, 2006). Therefore, kriging variance at long lags may be underestimated (by failing to include the uncertainty of the detrending model) or even overestimated (by biased sampling affecting the detrending model and failing to capture the minimum temporal variance in that region).

We model the variogram sill as the population variance, but clear mismatches in long-lag empirical variograms are apparent (Supplemental Figure S2), with some lag intervals having both much higher and much lower variance. In addition to a violation of first-order stationarity, we interpret this as a lack of knowledge of the structure of long-term $\delta^{34}S$ trends where it is not constrained by data, rather than a quantitative statement about its variance over long timescales. In other words, dramatic sulfur isotope excursions may be possible in unsampled intervals of geologic time, and there is no predictive power from the variance deriving from the amplitude of currently observed excursions. Our goal of using the kriged variance to describe the quality of $\delta^{34}S$ records is therefore critically different than using the kriged variance to predict $\delta^{34}S$ through time, in the way that kriging is often applied to predict spatial-temporal patterns in environmental and earth sciences.

On the other hand, the estimates of uncorrelated variance—that on short timescales—are generally well constrained by the data. For estimating kriging variance through time, the variogram model

at short lags is much more important than at long lags. Over the observed range of correlation until semivariance matches or exceed population variance, most records in each time period indeed show increasing semivariance with lag distance (Supporting Figure S2). Only one set of data, the Cenozoic bulk rock CAS record, has a negligible difference between uncorrelated and population variance. Constraints on either are therefore poor, but resultant kriging variance is insensitive to the exact shape of the variogram model.

Timeseries variography and kriging of synthetic data

Variography and kriging can usefully describe the structure of variance of timeseries $\delta^{34}S$ data. In addition to differences between the proxy records inherent to each geologic archive, some variance in the records may derive from misalignment of age models.

The dashed line in Supporting Figure S3a represents a synthetic isotope excursion similar in duration and magnitude to some reported in the Paleozoic, such as during the Cambrian SPICE interval (e.g., Gill et al., 2007). The orange dots represent samples taken randomly in time from a population that follows the synthetic excursion with synthetic Gaussian noise with a standard deviation of 2‰. The variogram captures a 1‰ 1σ standard deviation of uncorrelated variance at the shortest lag interval and approaches the population variance (*ca.* 5‰) of the synthetic data over a range of approximately 500 kyr. Applying a circular variogram model and kriging the random samples results in the gray kriged estimate.

But, given multiple aligned records, how much of the variogram structure is attributable to the inherent "noise" in the archive (illustrated in Supporting Figure S3a) and how much is attributable to poor temporal alignment? Supporting Figures S3b and S3c test this by overlaying the synthetic record in Supporting Figure S3a with randomly misaligned records. Supporting Figures S3b represents poor alignment of multiple identical records sampled at different localities by randomly misaligning the full excursion within the average length of a Paleozoic stage. Although the kriged estimate of the interpolated record and the variogram are clearly different than the true synthetic excursion, the uncorrelated variance and population variance are only slightly larger. These are robust statistical descriptions of the uncertainty in the data.

Similarly, an unconformity or uneven sedimentation rate may change the amplitude or shape of an isotope excursion if, when sampling, this is unknown. Supporting Figure S3c shows how randomly varying the amplitude of the excursion in Supporting Figure S3a with a standard deviation of 25% also does not dramatically increase the nugget or sill variance.

In summary, it is likely that the increase in both uncorrelated (nugget) and population (sill) variance of all records with age represents both poorer age control in older strata, and also a meaningful change in the variability of ancient rocks due to changes in how sulfate is incorporated and preserved.

Supporting Figures, Tables, and Files

Supporting Figure S1. *Histograms of $\delta^{34}S$ of sulfate in each proxy for ancient seawater sulfate with means and 1σ standard deviations. Arrows mark bins with 1 to 10 counts, and the broken line marks the means.*

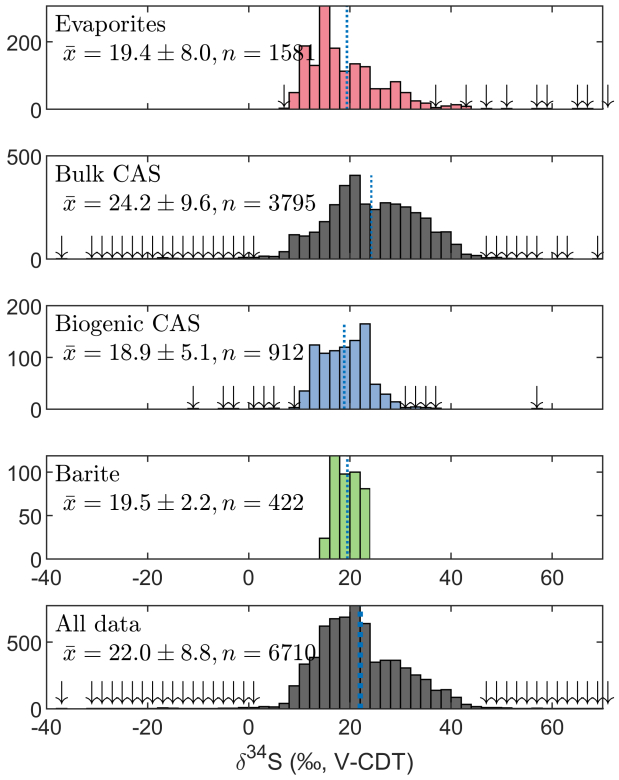

Supporting Figure S2. *Empirical variograms showing semivariance as a function of lag times less than 40 Myr for each record, and for each record by geologic age. The dashed horizontal line is the population variance of all data within the 1st and 99th percentile of the linearly detrended $\delta^{34}S$ data, which is used to estimate the sill for the circular variogram model (green solid line). The unresolved variance for each record is the semivariance at the shortest lag.*

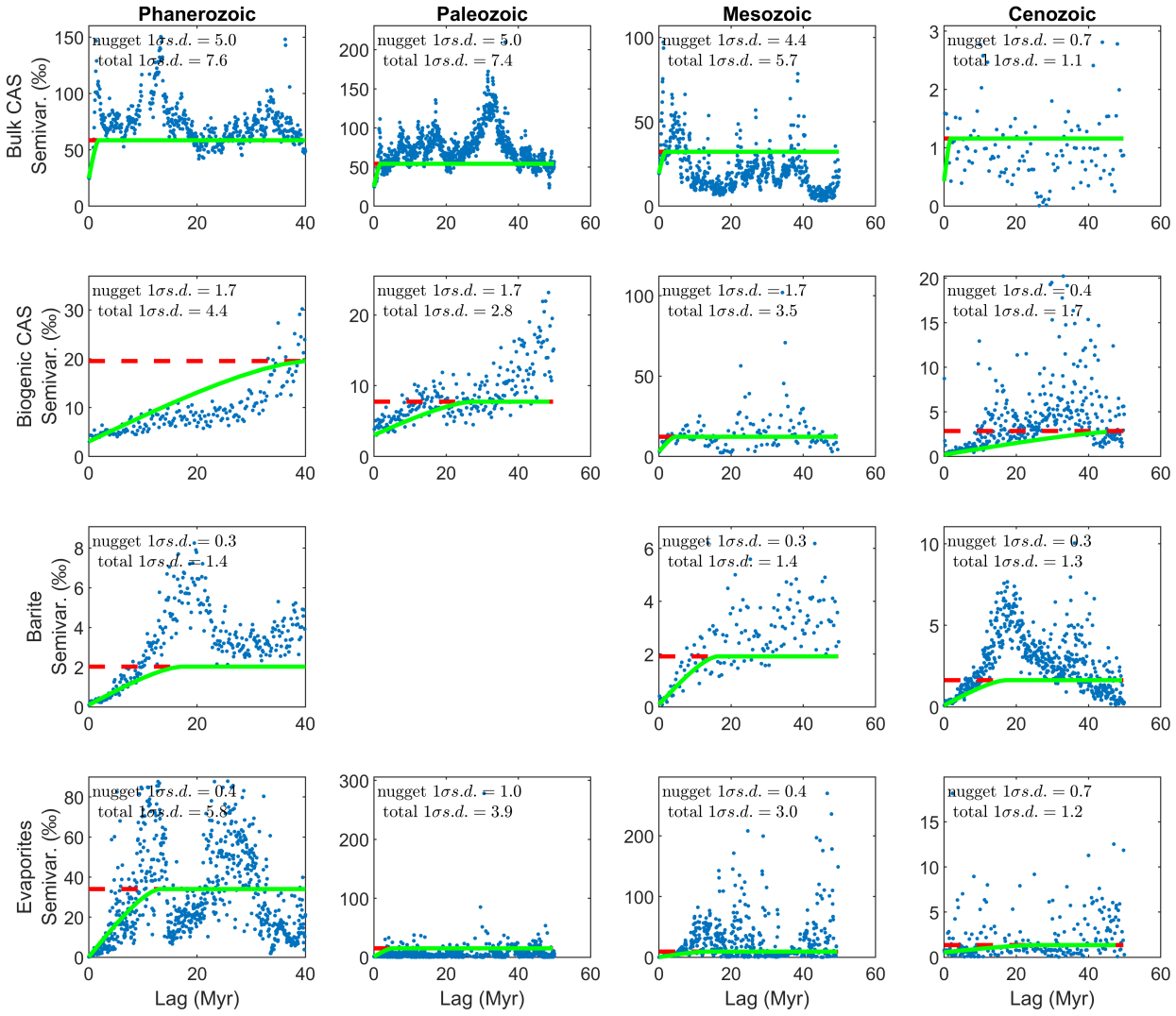

Supporting Figure S3. *Synthetic data to examine the effect sampling and age modelling on the variogram of a global isotope excursion sampled at multiple localities. All sampling and age model artifacts lead to less than 3‰ nugget effects, which may account for a source of unresolved variance in many proxy records but cannot explain all unresolved variance in the Phanerozoic.* ***(a)*** *Imprecise sampling represented by Gaussian noise with a standard deviation of 2‰ added to a synthetic $\delta^{34}S$ excursion with 20‰ amplitude over 2 Myr, like some Paleozoic excursions in CAS data.* ***(b)*** *Imprecise age alignment represented by precise sampling of multiple randomly aligned but otherwise identical excursions varying within the average length stratigraphic stage.* ***(c)*** *Inaccurate age model represented by randomly varying amplitude with 5‰ standard deviation, which is the effect of an unconformity of unknown duration adding 25% variability to the true excursion amplitude.*

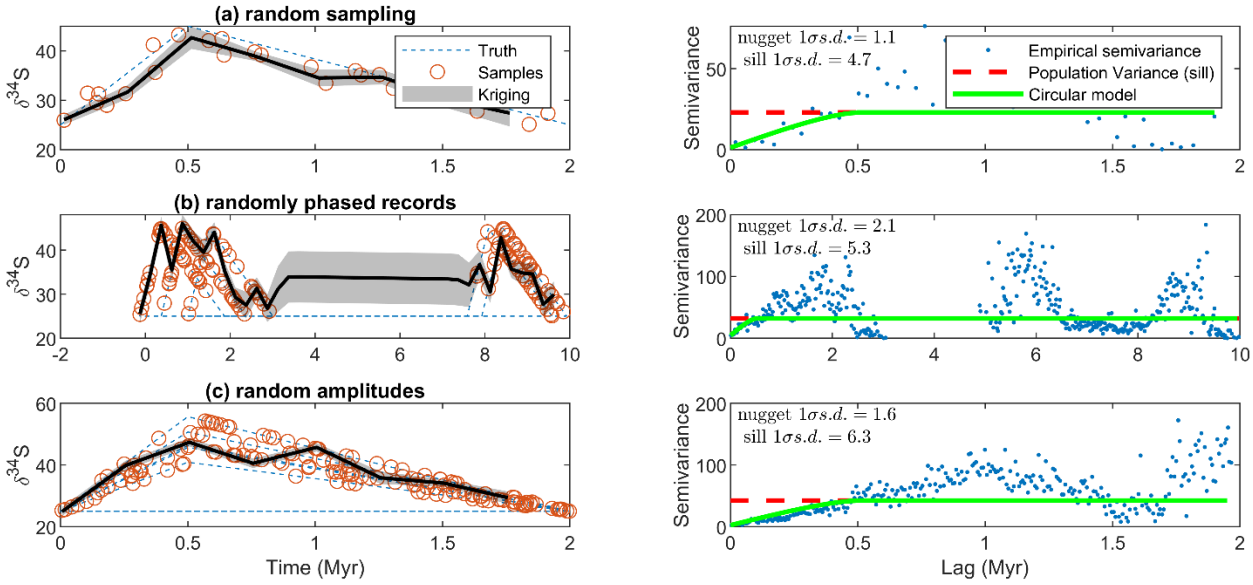

Supporting File d34S_Data.xlsx. *This Microsoft Excel spreadsheet contains all compiled $\delta^{34}S$ values, their assigned age, the proxy material from which they derive, and their source reference.*

Supporting Table S1. *Statistical description of all Phanerozoic $\delta^{34}S$ data. SD = standard deviation. CI = confidence interval.*

	n	mean	SD	median (95% CI)	skewness
Evaporite	1581	19.41	7.98	17.10 (16.76 – 17.44)	1.82
Biogenic CAS	912	18.87	5.14	18.80 (18.41 – 19.19)	0.28
Bulk CAS	3795	24.18	9.62	23.70 (23.38 – 24.02)	-0.48
Barite	422	19.50	2.22	19.15 (18.83 – 19.47)	-0.10
All data	*6710*	*22.04*	*8.79*	*21.08(20.86 – 21.30)*	*0.23*

Supporting Table S2. *References for $\delta^{34}S$ data included in compilation; number of CAS, evaporite, and barite analyses in each reference; and description of age assignments for the data.*

Reference	CAS	Evap.	Bar.	Age Model and Notes
Adams et al. (2010)	16			Ages linearly interpolated between Ar/Ar dates in provided in Figure 1 in paper. Stratigraphic heights extracted graphically.
Arp et al. (2008)	6			Assigned age of 146 Ma for the latest Tithonian
Ault & Kulp (1959)		12		Evaporite ages updated to latest stratigraphy. Omitted salt dome (migrated) samples from Feely & Kulp (1957), and only included samples with formation tabulated
Balderer et al. (1991)		11		Data compiled with age model by Bernasconi et al. (2017). Omitted vein and sandstone cement anhydrite samples.
Baldermann et al. (2015)	8			Linear interpoloation of stratigraphic height between Rb/Sr ages in paper
Bernasconi et al. (2017)		282		Age model provided in paper
Boschetti et al. (2011)		8		Data compiled with age model by Bernasconi et al. (2017)
Burdett et al. (1989)	56	25		Linear interpolation of stage boundaries from Berggren et al. (1985) to ICS2016/04 timescale. Ages and $\delta^{34}S$ extracted graphically from Figure 3.
Buschendorf et al. (1963)		24		Evaporites updated to latest stratigraphy. Omitted sulfide and barite samples.
Chen et al. (1981)		52		Translated from Chinese by Sang Chen, and $\delta^{34}S$ extracted graphically from figures. Only included Cambrian-Ordovician evaporites for which locality and unit could be determined.
Chen et al. (2013)	71			Linear interpolation of stratigraphic height between conodont zone age constraints from Kaufmann (2006), updated to GSSP ages in ICS2016/04
Claypool et al. (1980)		272		Evaporite ages updated to latest stratigraphy
Cortecci et al. (1981)		30		Used age model in Bernasconi et al. (2017), and assigned additional data from Western Alps to Rhaetian (Loprieno et al., 2011)
Dahl et al. (2019)	35			Ages provided in paper
Das et al. (1990)		6		Updated Michigan Basin chronostratigraphy from Rine et al. (2017)
Davies & Krouse (1975)		23		Evaporite ages updated to latest stratigraphy
Edwards et al. (2018)	117			Age model provided in paper
Fanlo & Ayora (1998)		26		Data compiled with age model by Bernasconi et al. (2017)
Fike & Grotzinger (2008)	157			Ages provided in Fike et al. (2015)
Fox & Videtich (1997)	13			Evaporite ages updated to latest Williston Basin stratigraphy using Taki & Pratt (2012)
Gill, Lyons, & Jenkyns (2011)	105			Linear interpolation of stratigraphic height between stage boundaries using ICS2016/04, assigning Calcari Maculati to Bajocian stage

Reference	CAS	Evap.	Bar.	Age Model and Notes
Gill, Lyons, Young, et al. (2011)	111			Linear interpolation of stratigraphic height between stage boundaries
Gill et al. (2007)	74			Linear interpolation of stratigraphic height between stage boundaries
Gomes et al. (2016)	115			Ages provided in paper on GTS2012 time scale, which matches ICS2016/04 in the Cretaceous
He et al. (2019)	165			Ages provided in paper for Siberian CAS data. For South China, age linearly interpolated by stratigraphic height between ICS2016/04 age of 529 Ma assigned to FAD of *W. crosby*i at base of Dahai Mbr, and age of 526.5 Ma to base of Shiyantou Fm. (Yang et al., 2018)
Hitchen & Krouse (1972)		6		Evaporite ages updated at stage scale to latest stratigraphy; omitted non-marine recent and migrated salt dome samples
Holser & Kaplan, Chem. Geol. (1966)		49		Evaporite ages updated to latest stratigraphy. Omitted salt dome (migrated) and secondary (cements/vugg-filling/intrusive igneous) textures
Horacek et al. (2010)		6		Data compiled with age model by Bernasconi et al. (2017)
Hovorka et al. (1993)		34		Assigned Delaware Basin ages from Wu et al. (2020) and Kerans and Tinker (1999). Data extracted graphically from Figure 5.
Hurtgen et al. (2009)	30			At Felix Cove, carbon isotope maxima in SPICE is set as base of Steptoean (Saltzman et al., 2004). In other sections, biomere event at onset of SPICE is set as base of Steptoean. March Pt. Formation includes *Bolaspidella* trilobites (Upper Middle Cambrian), and total deposition likely 5-10Ma; the lowest sample in the March Pt. Formation is set as the base of the Marjuman. Straigraphic heights extracted graphically.
Insalaco et al. (2006)		23		Age model provided by Bernasconi et al. (2017)
John et al. (2010)	34			Linear interpolation of stratigraphic height between conodont zone age constraints from Kaufmann (2006), updated to GSSP ages in ICS2016/04. Stratigraphic heights extracted from Fig. 4 and 5 graphically
Johnson et al. (in revision)	130			Ages provided in paper interpolated to ICS2016/04
Jones & Fike (2013)	42			Linearly interpolated between stage boundaries using ICS2016/04. Hirnantian and Ordovician-Silurian boundary placed based on carbon isotope stratigraphy, not biostratigraphy, in text.
Kah et al. (2016)	42			Ages provided in Fig 9, using ICS2016/04 ages at the tie points
Kaiho et al. (2006)	11			Approximated age model as described for Schobben et al. (2017)
Kaiho et al. (2001)	12			Meishan section bed ages and accumulation rates from Burgess et al. (2014). Data tabulated in Kaiho et al. (2006)
Kaiho et al. (1999)	18			K-Pg boundary set at ICS2016/04 age, and sedimentation rates from paper. Data extracted graphically from Figure 3

Reference	CAS	Evap.	Bar.	Age Model and Notes
Kampschulte & Strauss (2004)	244			Ages updated by interpolation to ICS2016/04 from Harland 1989 Timescale (Harland et al., 1990). Data tabulated in Kampschulte (2001) and Kampschulte et al. (2001)
Kramm & Wedopohl (1991)		9		Zechstein evaporites tied to ICS2016/04 using ~1Myr/unit starting at the bottom of the Lopingian (Stollhofen et al., 2008)
Korte et al. (2004)	5			18.5m correlated by Gorjan & Kaiho (2007) to 250.7 Ma age in Bowring et al. (1998); linearly interpolated with *H. Parvus* FAD from Burgess et al. (2014)
Kozik et al. (2019)	48			Ages provided in paper in Fig. 3 based on Sr isotope stratigraphy by Saltzman et al. (2004)
Li et al. (2009)	27			Bed 27/28 boundary is proposed Permian-Triassic Boundary; using age from Burgess et al. (2014). Maokou/Wujiaping Fm. boundary is Guadalupian-Lopingian Boundary according to Yadong et al. (2008); using age from ICS2016/04. Data extracted from figures graphically.
Longinelli & Flora (2007)		8		Data compiled with age model by Bernasconi et al. (2017)
Loyd et al. (2012)	63			Linear interpolation of stratigraphic height between stage boundaries using ICS2016/04
Lu & Meyers (2003)		16		Middle Messinian age assigned in ICS2016/04
Luo et al. (2010)	58			Base of microbialite in Cili section correlated to base of Bed 25 in Meishan, and assigned age from Burgess et al. (2014); linearly interpolated height with FAD of *H. Parvus* assigned age from Burgess et al. (2014)
Lyu et al. (2019)	126			Ages provided in Fig. 8
Maharjan et al. (2018)	59			Linear interpolation of GTS2012 age model for conodont biostratigraphy provided in Fig. 1
Marenco et al. (2008)	25	9		Section correlated using flooding surfaces and Sr isotope data, and linearly interpolating ages of the Spathian/Anisian and Smithian/Spathian boundaries from Burgess et al. (2014)
Marenco et al. (2013)	20			Linear interpolation of stratigraphic height using stratigraphy published in Marenco et al. (2016), which uses ages in ICS2016/04. Data table appears truncated in publication; stratigraphic height and $\delta^{34}S$ extracted graphically from Fig. 4
Marenco et al. (2016)	7			Linear interpolation of stratigraphic height between stage boundaries in Fig 2, using ages from Kah et al. (2016), which match ICS2016/04
Meng, Zhang, Yan, et al. (2019)		5		Kept middle/upper Darriwilian assignment consistent with biostratigraphy and carbon isotope stratigraphy
Meng, Zhang, Schiffbauer, et al. (2019)		12		Tarim basin trilobite stratigraphy from Zhu et al. (2019). Includes one Lower Ordovician data from Cai et al. (2001) constrained to Tremadocian (Guo et al., 2018).
Mills et al. (2017)	114			Age model developed in paper on GTS2012 time scale, which matches ICSv2016/04 in the Cretaceous

Reference	CAS	Evap.	Bar.	Age Model and Notes
Newton et al. (2004)	32			Linear interpolation of stratigraphic height over the extinction interval using ages from Burgess et al. (2014), and age of 251.5 Ma for top of Tesero Ooilite set as the age at which the $\delta^{13}C$ returns to a "flat" value at the Meishan GSSP
Newton et al. (2011)	85			Linear interpolation of stratigraphic height between stage boundaries using ICS2016/04 for Yorkshire section, and correlated Tibet strata using chemostratigraphy preferred by the authors
Nielsen & Ricke (1964)		51		Evaporite ages updated to latest stratigraphy. Omitted caprock, stratigraphically unconstrained samples, lacustrine and freshwater-influenced samples, and Mg and K sulfates
Ohkouchi et al. (1999)	27			Age model based on Al accumulation provided in paper, and shifted +0.29 Myr to agree with ICS2016/04 Cenomanian-Turonian boundary age of 93.9Ma. Ages and $\delta^{34}S$ extracted graphically from Fig. 3A.
Owens et al. (2013)	216			Eastbourne section sedimentation rates between carbon isotope excursion features from Voigt et al. (2008) astrochronology tied to ICS2016/04 time scale using Cenomanian-Turonian GSSP. South Ferriby and Trunch sections tied to ages of CIE calculated for Eastbourne section and linearly interpolated stratigraphic height. Raia del Pedale section height linearly interpolated between CIE ages from Eastbourne and stage boundaries.
Pankina et al. (1975)		18		Evaporite ages updated to latest stratigraphy
Paytan et al. (1998)			69	Ages updated to ICS2016/04 from those provided in Kurtz et al. (2003), which uses Berggren et al. (1995) timescale. Ages for Sites 305, 366, and 577 updated to ICS2016/04 from those provided in Yao et al. (2020).
Paytan et al. (2004)			123	Ages updated to GTS2004 by Prokoph et al. (2008), and then interpolated to ICS2016/04
Peryt et al. (2010)		52		Evaporite ages updated to latest stratigraphy
Pisarchik & Golubchina (1975)		17		Evaporite ages updated to latest stratigraphy; omitted Vendian Motyi Formation
Playà et al. (2007)		10		Age of 70 kyr given in text
Posey & Fisher (1989)		59		Assigned Kungarian to lowermost Roadian age to reconcile top-Wolfcamp correlations between Midland and Palo Duro basins (Blomquist, 2016; Handford & Dutton, 1980; Mazzullo, 1982). Interpolated correlated wells as in Fig. 3
Poulton et al. (2015)	24			Sedimentation rates from Kolonic et al. (2005), rescaled to reflect obliquity-controlled cycles instead of eccentricity, as the authors prefer, citing Meyers et al. (2012). Cenomanian-Turonian boundary shifted from GTS2004 age in Kolonic et al. (2005) to ICS2016/04.
Present et al. (2015)	77			Ages determined by linearly interpolating stage boundaries, which are placed with carbon isotope stratigraphy as described by Jones & Fike (2013)

Reference	CAS	Evap.	Bar.	Age Model and Notes
Present (2018, Ch. 3)	52			ICS2016/04 ages used to interpolate biostratigraphy and carbon isotope stratigraphy in Bergström et al (2009) and Cramer et al. (2010)
Present et al. (2019)	255			Linearly interpolated stratigraphic height between high frequency sequence boundary ages in Wu et al. (2020)
Rennie & Turchyn (2014)	56			Site 807A to 362.8m: Martin & Scher (2004); Site 807A below 362.8m: Schrag et al. (1995); Site 821A: Wei & Gartner (1993); Site 1003A: Wright & Kroon (2000)
Rennie et al. (2018)	119			Age model provided in paper
Riccardi et al. (2006)	102			Used Burgess et al. (2014) ages for Meishan section and extinction interval at Shangsi, and for Dienerian base. Used Algeo et al. (2013) age for Changhsingian base. Used Bowring et al. (1998) age for base of Meishan bed #7.
Richardson et al. (2019)	93			Linearly interpolated ages with stratigraphic height given in Fig. 4
Rose et al. (2019)	118			Linearly interpolated stratigraphic height between Datum 2 bentonite age of 431.8 Ma and top of Sheinwoodian Sub-stage 2 from Cramer et al. (2012)
Sakai (1972)		13		Evaporite ages updated to latest stratigraphy. Omitted Precambrian samples, and samples purposely chosen to have anomalously-low $\delta^{34}S$
Schobben et al. (2015)	74			Ages provided in paper using Burgess et al. (2014) dates
Schobben et al. (2017)	19			Assigned approximate mid-Griesbachian age of 251.50 Ma to uppermost Balvany East strata, and linearly interpolated stratigraphic height to Permian-Triassic Boundary at base of Gerennavar Fm., neglecting missing section between Balvany East and Balvany North; used same accumulation rate for limestones in Nagyvisnyo Fm. anchored at EPME and apportioned remaining time in the Boundary Shale beds between top of limestones and P-Tr. Boundary
Schroder et al. (2004)		29		Ages provided in Fike et al. (2015)
Sim et al. (2015)	68			Ages provided in paper using Kaufmann (2006) time scale updated to GSSP ages in ICS2016/04
Solomon et al. (1971)		27		Evaporite ages updated at stage scale to latest stratigraphy
Song et al. (2014)	202			Age model is from Figure 4 (tie points are in bold), using dates from Burgess et al. (2014) and ICS2016/04; interpolated linearly in between tie points; Composite height is linking of sections by the C-isotope tie points in Figures 3 and 4: Daijang 400m = Lower Guandau 135m (N3); Lower Guandau 225m = Upper Guandau 10m (P4). Adjusted Daijang B by 18m to approx. bring in line with Daijang A, as in Fig 3

Reference	CAS	Evap.	Bar.	Age Model and Notes
Song et al. (2019)	29			Age model tied to Song et al. (2014) using correlation in Fig. 8 by linearly apportioning height between 40m and 48m to gap at Smithian-Spathian Boundary between 139.2m and 163m at Lower Guandau, and Burgess et al. (2014) age for base of Smithian at base of section
Spötl (1988)		8		German-language data compiled and assigned ages by Bernasconi et al. (2017)
Stebbins et al. (2019)	75			Age model provided in Supplemental Figure S4
Thode & Monster (1965)		68		Evaporite ages updated to latest stratigraphy. Data is reported as the range of measurements, so only could include the maximum and minimum values in compilation; omitted poorly-constrained intervals.
Thode & Monster (1970)		17		Evaporite ages updated at stage scale to latest stratigraphy
Thode et al. (1958)		5		Assigned to upper Frasnian (Hearn et al., 2011)
Thompson & Kah (2012)	235			Ages provided in paper using U/Pb dates in Thompson et al. (2012). Data tabulated in Thompson (2011).
Turchyn et al. (2009)	39		39	Ages updated by interpolation to ICS2016/04 from GTS2004
Utrilla et al. (1992)		62		Listed formations assigned by stage to ICS2016/04 ages. Omitted continental evaporite formations.
van Everdingen et al. (1982)		70		Evaporite ages updated to latest stratigraphy. Omitted vein gypsum.
Vinogradov (2007)		23		Toyonian evaporites assigned in 1 Myr intervals by subformation (Novikov, 2017)
Vredenburgh & Cheney (1971)		16		Evaporite ages updated to latest stratigraphy. Omitted "sulfur crusts."
Witts et al. (2018)	41			Linearly interpolated magnetochronological age assignments using stratigraphic heights.
Worden et al. (1997)		11		Used age model in Bernasconi et al. (2017)
Wotte et al. (2012)	85			Linear interpolation of stratigraphic height between stage boundaries
Wotte et al. (2011)	69			Linear interpolation of stratigraphic height between stage boundaries, using Susan Duster Limestone sedimentation rate for Molodo River and Ulakhan-Kyyry-Taas sections
Wu et al. (2014)	214		66	Ages updated by interpolation to ICS2016/04 from GTS2004. Data tabulated in Wu (2013).
Yan et al. (2013)	27			Guadalupian-Lopingian boundary set at base of *C.p.p.* based on ICS2016/04; Sedimentation rate from Qiu et al. (2015) indicate 0.04cm/kyr in the bedded chert relative to bentonite (257 Ma) at top of *C.p.p* zone, so base of bedded chert is 258.6 Ma.; applied this sed rate down through the limestone
Yao et al. (2018)			58	Age model provided in paper relative to PETM, which is taken as 55.93 Ma after Westerhold et al. (2008)
Yao et al. (2020)			88	Ages updated by interpolation to ICS2016/04 from GTS2012

Reference	CAS	Evap.	Bar.	Age Model and Notes
Yeremenko & Pankina (1972)		17		Evaporite ages updated to latest stratigraphy
Young et al. (2016)	68			Linear interpolation of stratigraphic height between stage boundaries in Fig 2 and 3
Young et al. (2019)	40			Assigned base and top of Ireviken CIE to bentonite age of 431.8 Ma and top of Sheinwoodian Sub-stage 2 (430.2 Ma) from Cramer et al. (2012) for Roberts Mtn. section. Aligned Newsom Roadcut carbon isotope record with Roberts Mtn. section, with unconformity on rising limb
Zhang et al. (2015)	15			Used Smithian/Spathian boundary ages from Burgess et al. (2014) and sedimentation rates provided in Figure 3

Supporting References

Adams, D. D., Hurtgen, M. T., & Sageman, B. B. (2010). Volcanic triggering of a biogeochemical cascade during Oceanic Anoxic Event 2. *Nature Geoscience*, *3*(3), 201–204. https://doi.org/10.1038/Ngeo743

Algeo, T. J., Henderson, C. M., Tong, J., Feng, Q., Yin, H., & Tyson, R. V. (2013). Plankton and productivity during the Permian–Triassic boundary crisis: An analysis of organic carbon fluxes. *Global and Planetary Change*, *105*, 52–67. https://doi.org/10.1016/j.gloplacha.2012.02.008

Arp, G., Ostertag-Henning, C., YÜCekent, S., Reitner, J., & Thiel, V. (2008). Methane-related microbial gypsum calcitization in stromatolites of a marine evaporative setting (Münder Formation, Upper Jurassic, Hils Syncline, north Germany). *Sedimentology*, *55*(5), 1227–1251. https://doi.org/10.1111/j.1365-3091.2007.00944.x

Ault, W. U., & Kulp, J. L. (1959). Isotopic geochemistry of sulphur. *Geochimica et Cosmochimica Acta*, *16*(4), 201–235. https://doi.org/10.1016/0016-7037(59)90112-7

Balderer, W., Pearson, F. J., & Soreau, S. (1991). Formation-Specific Characterization of Groundwaters. In F. J. Pearson, W. Balderer, H. H. Loosli, B. E. Lehmann, A. Matter, T. Peters, et al. (Eds.), *Applied Isotope Hydrogeology: A Case Study in Northern Switzerland: Technical Report 88-01* (pp. 297–374). Amsterdam: Elsevier. Retrieved from https://books.google.com/books?id=fEBs7PudzAEC

Baldermann, A., Deditius, A. P., Dietzel, M., Fichtner, V., Fischer, C., Hippler, D., et al. (2015). The role of bacterial sulfate reduction during dolomite precipitation: Implications from Upper Jurassic platform carbonates. *Chemical Geology*, *412*, 1–14. https://doi.org/10.1016/j.chemgeo.2015.07.020

Berggren, W. A., Kent, D. V., Flynn, J. J., & Van Couvering, J. A. (1985). Cenozoic geochronology. *Geological Society of America Bulletin*, *96*, 1407–1418.

Berggren, W. A., Kent, D. V., Swisher, C. C., & Aubry, M.-P. (1995). A Revised Cenozoic Geochronology and Chronostratigraphy. In *Geochronology, Time Scales and Global Stratigraphic Correlation* (pp. 129–212). SEPM (Society for Sedimentary Geology). https://doi.org/10.2110/pec.95.04.0129

Bergström, S. M., Chen, X., Gutiérrez-Marco, J. C., & Dronov, A. (2009). The new chronostratigraphic classification of the Ordovician System and its relations to major regional series and stages and to δ13C chemostratigraphy. *Lethaia*, *42*(1), 97–107. https://doi.org/10.1111/j.1502-3931.2008.00136.x

Bernasconi, S. M., Meier, I., Wohlwend, S., Brack, P., Hochuli, P. A., Bläsi, H., et al. (2017). An evaporite-based high-resolution sulfur isotope record of Late Permian and Triassic seawater sulfate. *Geochimica et Cosmochimica Acta*, *204*, 331–349. https://doi.org/10.1016/j.gca.2017.01.047

Blomquist, P. K. (2016). Wolfcamp Horizontal Play, Midland Basin, West Texas, #10890 (2016). In *AAPG Pacific Section and Rocky Mountain Section Joint Meeting* (p. 34). Las Vegas, Nevada. Retrieved from http://www.searchanddiscovery.com/pdfz/documents/2016/10890blomquist/ndx_blomquist.pdf.html

Boschetti, T., Cortecchi, G., Toscani, L., & Iacumin, P. (2011). Sulfur and oxygen isotope compositions of Upper Triassic sulfates from Northerm Apennines (Italy): palaeogeographic and hidrogeochemical implications. *Geologica Acta*, *9*(2), 129–147. https://doi.org/10.1344/105.000001690

Bowring, S. A., Erwin, D. H., Jin, Y. G., Martin, M. W., Davidek, K., & Wang, W. (1998). U/Pb Zircon Geochronology and Tempo of the End-Permian Mass Extinction. *Science*, *280*(5366), 1039–1045. https://doi.org/10.1126/science.280.5366.1039

Burdett, J. W., Arthur, M. A., & Richardson, M. (1989). A Neogene seawater sulfur isotope age curve from calcareous pelagic microfossils. *Earth and Planetary Science Letters*, *94*, 189–198. https://doi.org/10.1016/0012-821x(89)90138-6

Burgess, S. D., Bowring, S., & Shen, S. (2014). High-precision timeline for Earth's most severe extinction. *Proceedings of the National Academy of Sciences*. https://doi.org/10.1073/pnas.1317692111

Buschendorf, Fr., Nielsen, H., Puchelt, H., & Ricke, W. (1963). Schwefel-Isotopen-Untersuchungen am Pyrit-Sphalerit-Baryt-Lager Meggen/Lenne (Deutschland) und an verschiedenen Devon-Evaporiten. *Geochimica et Cosmochimica Acta*, *27*(5), 501–523. https://doi.org/10.1016/0016-7037(63)90085-1

Cai, C., Hu, W., & Worden, R. H. (2001). Thermochemical sulphate reduction in Cambro–Ordovician carbonates in Central Tarim. *Marine and Petroleum Geology*, *18*(6), 729–741. https://doi.org/10.1016/S0264-8172(01)00028-9

Chen, D., Wang, J., Racki, G., Li, H., Wang, C., Ma, X., & Whalen, M. T. (2013). Large sulphur isotopic perturbations and oceanic changes during the Frasnian–Famennian transition of the Late Devonian. *Journal of the Geological Society*, *170*(3), 465–476. https://doi.org/10.1144/jgs2012-037

Chen, J., Zhao, R., Huo, W., Yao Yuyuan Pan, S., Shao, M., & Hai, C. (1981). Sulfur Isotopes of Some Marine Gypsum. *Chinese Journal of Geology*, *3*, 009.

Claypool, G. E., Holser, W. T., Kaplan, I. R., Sakai, H., & Zak, I. (1980). The age curves of sulfur and oxygen isotopes in marine sulfate and their mutual interpretation. *Chemical Geology*, *28*, 199–260. https://doi.org/10.1016/0009-2541(80)90047-9

Cortecci, G., Reyes, E., Berti, G., & Casati, P. (1981). Sulfur and oxygen isotopes in Italian marine sulfates of Permian and Triassic ages. *Chemical Geology*, *34*(1), 65–79. https://doi.org/10.1016/0009-2541(81)90072-3

Cramer, B. D., Loydell, D. K., Samtleben, C., Munnecke, A., Kaljo, D., Männik, P., et al. (2010). Testing the limits of Paleozoic chronostratigraphic correlation via high-resolution (<500 k.y.) integrated conodont, graptolite, and carbon isotope (δ13Ccarb) biochemostratigraphy across the Llandovery–Wenlock (Silurian) boundary: Is a unified Phanerozoic time scale achievable? *Geological Society of America Bulletin*, 17.

Cramer, B. D., Condon, D. J., Söderlund, U., Marshall, C., Worton, G. J., Thomas, A. T., et al. (2012). U-Pb (zircon) age constraints on the timing and duration of Wenlock (Silurian) paleocommunity collapse and recovery during the "Big Crisis." *GSA Bulletin*, *124*(11–12), 1841–1857. https://doi.org/10.1130/B30642.1

Cressie, N., & Hawkins, D. M. (1980). Robust estimation of the variogram: I. *Journal of the International Association for Mathematical Geology*, *12*(2), 115–125. https://doi.org/10.1007/BF01035243

Dahl, T. W., Connelly, J. N., Li, D., Kouchinsky, A., Gill, B. C., Porter, S., et al. (2019). Atmosphere–ocean oxygen and productivity dynamics during early animal radiations. *Proceedings of the National Academy of Sciences*, *116*(39), 19352–19361. https://doi.org/10.1073/pnas.1901178116

Das, N., Horita, J., & Holland, H. D. (1990). Chemistry of fluid inclusions in halite from the Salina Group of the Michigan basin: Implications for Late Silurian seawater and the origin of sedimentary brines. *Geochimica et Cosmochimica Acta*, *54*(2), 319–327. https://doi.org/10.1016/0016-7037(90)90321-B

Davies, G. R., & Krouse, H. R. (1975). Sulphur isotope distribution in Paleozoic sulphate evaporites, Canadian Arctic Archipelago. *Geological Survey of Canada Paper*, *75–1 Part B*, 221–225.

Edwards, C. T., Fike, D. A., Saltzman, M. R., Lu, W., & Lu, Z. (2018). Evidence for local and global redox conditions at an Early Ordovician (Tremadocian) mass extinction. *Earth and Planetary Science Letters*, *481*, 125–135. https://doi.org/10.1016/j.epsl.2017.10.002

van Everdingen, R. O., Shakur, M. A., & Krouse, H. R. (1982). 34S and 18O abundances differentiate Upper Cambrian and Lower Devonian gypsum-bearing units, District of Mackenzie, N.W.T.—an update. *Canadian Journal of Earth Sciences*, *19*(6), 1246–1254. https://doi.org/10.1139/e82-106

Fanlo, I., & Ayora, C. (1998). The evolution of the Lorraine evaporite basin: implications for the chemical and isotope composition of the Triassic ocean. *Chemical Geology*, *146*(3), 135–154. https://doi.org/10.1016/S0009-2541(98)00007-2

Feely, H. W., & Kulp, J. L. (1957). Origin of Gulf Coast Salt-Dome Sulphur Deposits. *AAPG Bulletin*, *41*(8), 1802–1853.

Fike, D. A., & Grotzinger, J. P. (2008). A paired sulfate–pyrite δ34S approach to understanding the evolution of the Ediacaran–Cambrian sulfur cycle. *Geochimica et Cosmochimica Acta*, *72*(11), 2636–2648. https://doi.org/10.1016/j.gca.2008.03.021

Fike, D. A., Bradley, A. S., & Rose, C. V. (2015). Rethinking the Ancient Sulfur Cycle. *Annual Review of Earth and Planetary Sciences*, *43*(1), 593–622. https://doi.org/10.1146/annurev-earth-060313-054802

Fox, J. S., & Videtich, P. E. (1997). Revised estimate of δ34S for marine sulfates from the Upper Ordovician: data from the Williston Basin, North Dakota, U.S.A. *Applied Geochemistry*, *12*(1), 97–103. https://doi.org/10.1016/S0883-2927(96)00065-0

Gebbers, R. (2010). Geostatistics and Kriging. In M. H. Trauth, *MATLAB Recipes for Earth Sciences* (3rd Ed., pp. 235–254). Berlin, Germany: Springer-Verlag.

Gill, B. C., Lyons, T. W., & Saltzman, M. R. (2007). Parallel, high-resolution carbon and sulfur isotope records of the evolving Paleozoic marine sulfur reservoir. *Palaeogeography, Palaeoclimatology, Palaeoecology*, *256*, 156–173. https://doi.org/10.1016/j.palaeo.2007.02.030

Gill, B. C., Lyons, T. W., & Jenkyns, H. C. (2011). A global perturbation to the sulfur cycle during the Toarcian Oceanic Anoxic Event. *Earth and Planetary Science Letters*, *312*, 484–496. https://doi.org/10.1016/j.epsl.2011.10.030

Gill, B. C., Lyons, T. W., Young, S. A., Kump, L. R., Knoll, A. H., & Saltzman, M. R. (2011). Geochemical evidence for widespread euxinia in the Later Cambrian ocean. *Nature*, *469*, 80–83.

Gomes, M. L., Hurtgen, M. T., & Sageman, B. B. (2016). Biogeochemical sulfur cycling during Cretaceous oceanic anoxic events: A comparison of OAE1a and OAE2. *Paleoceanography*, *31*(2), 2015PA002869. https://doi.org/10.1002/2015PA002869

Gorjan, P., & Kaiho, K. (2007). Correlation and comparison of seawater δ34Ssulfate records at the Permian-Triassic transition. *Chemical Geology*, *243*, 275–285. https://doi.org/10.1016/j.chemgeo.2007.03.011

Guo, C., Chen, D., Song, Y., Zhou, X., Ding, Y., & Zhang, G. (2018). Depositional environments and cyclicity of the Early Ordovician carbonate ramp in the western Tarim Basin (NW China). *Journal of Asian Earth Sciences*, *158*, 29–48. https://doi.org/10.1016/j.jseaes.2018.02.006

Handford, C. R., & Dutton, S. P. (1980). Pennsylvanian–Early Permian Depositional Systems and Shelf-Margin Evolution, Palo Duro Basin, Texas. *AAPG Bulletin*, *64*(1), 88–106. https://doi.org/10.1306/2F918932-16CE-11D7-8645000102C1865D

Harland, W., Armstrong, R., Cox, A., Craig, L., Smith, A., & Smith, D. (1990). *A Geologic Time Scale 1989*. Cambridge University Press.

He, T., Zhu, M., Mills, B. J. W., Wynn, P. M., Zhuravlev, A. Y., Tostevin, R., et al. (2019). Possible links between extreme oxygen perturbations and the Cambrian radiation of animals. *Nature Geoscience*, 1. https://doi.org/10.1038/s41561-019-0357-z

Hearn, M. R., Machel, H. G., & Rostron, B. J. (2011). Hydrocarbon breaching of a regional aquitard: The Devonian Ireton Formation, Bashaw area, Alberta, Canada. *AAPG Bulletin*, *95*(6), 1009–1037. https://doi.org/10.1306/09271010050

Hitchon, B., & Krouse, H. R. (1972). Hydrogeochemistry of the surface waters of the Mackenzie River drainage basin, Canada—III. Stable isotopes of oxygen, carbon and sulphur. *Geochimica et Cosmochimica Acta*, *36*(12), 1337–1357. https://doi.org/10.1016/0016-7037(72)90066-X

Holser, W. T., & Kaplan, I. R. (1966). Isotope geochemistry of sedimentary sulfates. *Chemical Geology*, *1*, 93–135. https://doi.org/10.1016/0009-2541(66)90011-8

Horacek, M., Brandner, R., Richoz, S., & Povoden-Karadeniz, E. (2010). Lower Triassic sulphur isotope curve of marine sulphates from the Dolomites, N-Italy. *Palaeogeography, Palaeoclimatology, Palaeoecology*, *290*(1), 65–70. https://doi.org/10.1016/j.palaeo.2010.02.016

Hovorka, S. D., Knauth, L. P., Fisher, R. S., & Gao, G. (1993). Marine to nonmarine facies transition in Permian evaporites of the Palo Duro Basin, Texas: Geochemical response. *GSA Bulletin*, *105*(8), 1119–1134. https://doi.org/10.1130/0016-7606(1993)105<1119:MTNFTI>2.3.CO;2

Hurtgen, M. T., Pruss, S. B., & Knoll, A. H. (2009). Evaluating the relationship between the carbon and sulfur cycles in the later Cambrian ocean: An example from the Port au Port Group, western Newfoundland, Canada. *Earth and Planetary Science Letters*, *281*(3–4), 288–297. https://doi.org/10.1016/j.epsl.2009.02.033

Insalaco, E., Virgone, A., Courme, B., Gaillot, J., Kamali, M., Moallemi, A., et al. (2006). Upper Dalan Member and Kangan Formation between the Zagros Mountains and offshore Fars, Iran: depositional system, biostratigraphy and stratigraphic architecture. *GeoArabia*, *11*(2), 75–176.

John, E. H., Wignall, P. B., Newton, R. J., & Bottrell, S. H. (2010). δ34SCAS and δ18OCAS records during the Frasnian–Famennian (Late Devonian) transition and their bearing on mass extinction models. *Chemical Geology*, *275*(3–4), 221–234. https://doi.org/10.1016/j.chemgeo.2010.05.012

Johnson, D. J., Grossman, E. L., & Adkins, J. F. (in revision). Single-brachiopod δ34SCAS indicates a dynamic, climate-influenced Permo-Carboniferous S cycle. *Earth and Planetary Science Letters*.

Jones, D. S., & Fike, D. A. (2013). Dynamic sulfur and carbon cycling through the end-Ordovician extinction revealed by paired sulfate–pyrite δ34S. *Earth and Planetary Science Letters*, *363*, 144–155.

Kah, L. C., Thompson, C. K., Henderson, M. A., & Zhan, R. (2016). Behavior of marine sulfur in the Ordovician. *Palaeogeography, Palaeoclimatology, Palaeoecology*, *458*, 133–153. https://doi.org/10.1016/j.palaeo.2015.12.028

Kaiho, K., Kajiwara, Y., Nakano, T., Miura, Y., Kawahata, H., Tazaki, K., et al. (2001). End-Permian catastrophe by a bolide impact: Evidence of a gigantic release of sulfur from the mantle. *Geology*, *29*, 815–818. https://doi.org/10.1130/0091-7613(2001)029<0815:epcbab>2.0.co;2

Kaiho, Kunio, Kajiwara, Y., Tazaki, K., Ueshima, M., Takeda, N., Kawahata, H., et al. (1999). Oceanic primary productivity and dissolved oxygen levels at the Cretaceous/Tertiary boundary: their decrease, subsequent warming, and recovery. *Paleoceanography*, *14*(4), 511–524.

Kaiho, Kunio, Kajiwara, Y., Chen, Z.-Q., & Gorjan, P. (2006). A sulfur isotope event at the end of the Permian. *Chemical Geology*, *235*(1–2), 33–47. https://doi.org/10.1016/j.chemgeo.2006.06.001

Kampschulte, A., & Strauss, H. (2004). The sulfur isotopic evolution of Phanerozoic seawater based on the analysis of structurally substituted sulfate in carbonates. *Chemical Geology*, *204*, 255–286. https://doi.org/10.1016/j.chemgeo.2003.11.013

Kampschulte, A., Bruckschen, P., & Strauss, H. (2001). The sulphur isotopic composition of trace sulphates in Carboniferous brachiopods: implications for coeval seawater, correlation with other geochemical cycles and isotope stratigraphy. *Chemical Geology*, *175*, 149–173. https://doi.org/10.1016/s0009-2541(00)00367-3

Kampschulte, Anke. (2001). *Schwefelisotopenuntersuchungen an strukturell substituierten Sulfaten in marinen Karbonaten des Phanerozoikums : Implikationen für die geochemische Evolution des Meerwassers und die Korrelation verschiedener Stoffkreisläufe*. Ruhr-Universität Bochum. Retrieved from http://www-brs.ub.ruhr-uni-bochum.de/netahtml/HSS/Diss/KampschulteAnke/

Kaufmann, B. (2006). Calibrating the Devonian Time Scale: A synthesis of U–Pb ID–TIMS ages and conodont stratigraphy. *Earth-Science Reviews*, *76*(3–4), 175–190. https://doi.org/10.1016/j.earscirev.2006.01.001

Kerans, C., & Tinker, S. W. (1999). Extrinsic stratigraphic controls on development of the Capitan Reef Complex. In A. H. Saller, P. M. Harris, B. L. Kirkland, & S. J. Mazzullo (Eds.), *Geologic Framework of the Capitan Reef*. Tulsa, Oklahoma: SEPM (Society for Sedimentary Geology).

Kolonic, S., Wagner, T., Forster, A., Sinninghe Damsté, J. S., Walsworth-Bell, B., Erba, E., et al. (2005). Black shale deposition on the northwest African Shelf during the Cenomanian/Turonian oceanic anoxic

event: Climate coupling and global organic carbon burial: BLACK SHALE DEPOSITION DURING THE CENOMA. *Paleoceanography*, *20*(1), n/a-n/a. https://doi.org/10.1029/2003PA000950

Korte, C., Kozur, H., Joachimski, M., Strauss, H., Veizer, J., & Schwark, L. (2004). Carbon, sulfur, oxygen and strontium isotope records, organic geochemistry and biostratigraphy across the Permian/Triassic boundary in Abadeh, Iran. *International Journal of Earth Sciences*, *93*(4), 565–581. https://doi.org/10.1007/s00531-004-0406-7

Kozik, N. P., Young, S. A., Bowman, C. N., Saltzman, M. R., & Them, T. R. (2019). Middle–Upper Ordovician (Darriwilian–Sandbian) paired carbon and sulfur isotope stratigraphy from the Appalachian Basin, USA: Implications for dynamic redox conditions spanning the peak of the Great Ordovician Biodiversification Event. *Palaeogeography, Palaeoclimatology, Palaeoecology*, *520*, 188–202. https://doi.org/10.1016/j.palaeo.2019.01.032

Kramm, U., & Wedepohl, K. H. (1991). The isotopic composition of strontium and sulfur in seawater of Late Permian (Zechstein) age. *Chemical Geology*, *90*(3), 253–262. https://doi.org/10.1016/0009-2541(91)90103-X

Kurtz, A. C., Kump, L. R., Arthur, M. A., Zachos, J. C., & Paytan, A. (2003). Early Cenozoic decoupling of the global carbon and sulfur cycles. *Paleoceanography*, *18*(4), 1090. https://doi.org/10.1029/2003PA000908

Lark, R. M., & Webster, R. (2006). Geostatistical mapping of geomorphic variables in the presence of trend. *Earth Surface Processes and Landforms*, *31*(7), 862–874. https://doi.org/10.1002/esp.1296

Li, P., Huang, J., Chen, M., & Bai, X. (2009). Coincident negative shifts in sulfur and carbon isotope compositions prior to the end-Permian mass extinction at Shangsi Section of Guangyuan, South China. *Frontiers of Earth Science in China*, *3*(1), 51–56. https://doi.org/10.1007/s11707-009-0018-4

Longinelli, A., & Flora, O. (2007). Isotopic composition of gypsum samples of Permian and Triassic age from the north-eastern Italian Alps: Palaeoenvironmental implications. *Chemical Geology*, *245*(3), 275–284. https://doi.org/10.1016/j.chemgeo.2007.08.009

Loprieno, A., Bousquet, R., Bucher, S., Ceriani, S., Dalla Torre, F. H., Fügenschuh, B., & Schmid, S. M. (2011). The Valais units in Savoy (France): a key area for understanding the palaeogeography and the tectonic evolution of the Western Alps. *International Journal of Earth Sciences*, *100*(5), 963–992. https://doi.org/10.1007/s00531-010-0595-1

Loyd, S. J., Marenco, P. J., Hagadorn, J. W., Lyons, T. W., Kaufman, A. J., Sour-Tovar, F., & Corsetti, F. A. (2012). Sustained low marine sulfate concentrations from the Neoproterozoic to the Cambrian: Insights from carbonates of northwestern Mexico and eastern California. *Earth and Planetary Science Letters*, *339–340*(0), 79–94. https://doi.org/10.1016/j.epsl.2012.05.032

Lu, F. H., & Meyers, W. J. (2003). Sr, S, and OSO4 Isotopes and the Depositional Environments of the Upper Miocene Evaporites, Spain. *Journal of Sedimentary Research*, *73*(3), 444–450. https://doi.org/10.1306/093002730444

Luo, G., Kump, L. R., Wang, Y., Tong, J., Arthur, M. A., Yang, H., et al. (2010). Isotopic evidence for an anomalously low oceanic sulfate concentration following end-Permian mass extinction. *Earth and Planetary Science Letters*, *300*(1–2), 101–111. https://doi.org/10.1016/j.epsl.2010.09.041

Lyu, Z., Zhang, L., Algeo, T. J., Zhao, L., Chen, Z.-Q., Li, C., et al. (2019). Global-ocean circulation changes during the Smithian–Spathian transition inferred from carbon-sulfur cycle records. *Earth-Science Reviews*. https://doi.org/10.1016/j.earscirev.2019.01.010

Maharjan, D., Jiang, G., Peng, Y., & Nicholl, M. J. (2018). Sulfur isotope change across the Early Mississippian K–O (Kinderhookian–Osagean) δ 13 C excursion. *Earth and Planetary Science Letters*, *494*, 202–215. https://doi.org/10.1016/j.epsl.2018.04.043

Marenco, P. J., Corsetti, F. A., Kaufman, A. J., & Bottjer, D. J. (2008). Environmental and diagenetic variations in carbonate associated sulfate: An investigation of CAS in the Lower Triassic of the western USA. *Geochimica et Cosmochimica Acta*, *72*, 1570–1582.

Marenco, Pedro J., Marenco, K. N., Lubitz, R. L., & Niu, D. (2013). Contrasting long-term global and short-term local redox proxies during the Great Ordovician Biodiversification Event: A case study from

Fossil Mountain, Utah, USA. *Palaeogeography, Palaeoclimatology, Palaeoecology*, *377*, 45–51. https://doi.org/10.1016/j.palaeo.2013.03.007

Marenco, Pedro J., Martin, K. R., Marenco, K. N., & Barber, D. C. (2016). Increasing global ocean oxygenation and the Ordovician Radiation: Insights from Th/U of carbonates from the Ordovician of western Utah. *Palaeogeography, Palaeoclimatology, Palaeoecology*, *458*, 77–84. https://doi.org/10.1016/j.palaeo.2016.05.014

Martin, E. E., & Scher, H. D. (2004). Preservation of seawater Sr and Nd isotopes in fossil fish teeth: bad news and good news. *Earth and Planetary Science Letters*, *220*(1), 25–39. https://doi.org/10.1016/S0012-821X(04)00030-5

Mazzullo, S. J. (1982). Stratigraphy and Depositional Mosaics of Lower Clear Fork and Wichita Groups (Permian), Northern Midland Basin, Texas. *AAPG Bulletin*, *66*(2), 210–227. https://doi.org/10.1306/03B59A67-16D1-11D7-8645000102C1865D

Meng, F.-W., Zhang, Z., Yan, X., Ni, P., Liu, W.-H., Fan, F., & Xie, G.-W. (2019). Stromatolites in Middle Ordovician carbonate–evaporite sequences and their carbon and sulfur isotopes stratigraphy, Ordos Basin, northwestern China. *Carbonates and Evaporites*, *34*(1), 11–20. https://doi.org/10.1007/s13146-017-0367-0

Meng, F.-W., Zhang, Z., Schiffbauer, J. D., Zhuo, Q., Zhao, M., Ni, P., et al. (2019). The Yudomski event and subsequent decline: new evidence from δ34S data of lower and middle Cambrian evaporites in the Tarim Basin, western China. *Carbonates and Evaporites*, *34*(3), 1117–1129. https://doi.org/10.1007/s13146-017-0407-9

Meyers Stephen R., Sageman Bradley B., & Arthur Michael A. (2012). Obliquity forcing of organic matter accumulation during Oceanic Anoxic Event 2. *Paleoceanography*, *27*(3). https://doi.org/10.1029/2012PA002286

Mills, J. V., Gomes, M. L., Kristall, B., Sageman, B. B., Jacobson, A. D., & Hurtgen, M. T. (2017). Massive volcanism, evaporite deposition, and the chemical evolution of the Early Cretaceous ocean. *Geology*, *45*(5), 475–478. https://doi.org/10.1130/G38667.1

Newton, R. J., Pevitt, E. L., Wignall, P. B., & Bottrell, S. H. (2004). Large shifts in the isotopic composition of seawater sulphate across the Permo–Triassic boundary in northern Italy. *Earth and Planetary Science Letters*, *218*, 331–345. https://doi.org/10.1016/S0012-821X(03)00676-9

Newton, R. J., Reeves, E. P., Kafousia, N., Wignall, P. B., Bottrell, S. H., & Sha, J. (2011). Low marine sulfate concentrations and the isolation of the European epicontinental sea during the Early Jurassic. *Geology*, *39*, 7–10. https://doi.org/10.1130/g31326.1

Nielsen, H., & Ricke, W. (1964). Schwefel-isotopen verhältnisse von evaporiten aus deutschland; Ein beitrag zur kenntnis von δ34S im meerwasser-sulfat. *Geochimica et Cosmochimica Acta*, *28*(5), 577–591. https://doi.org/10.1016/0016-7037(64)90078-X

Novikov, D. A. (2017). Distribution of Cambrian salts in the western Siberian craton (Yurubcheno-Tokhomo field, Russia). *Arabian Journal of Geosciences*, *10*(1). https://doi.org/10.1007/s12517-016-2792-0

Ohkouchi, N., Kawamura, K., Kajiwara, Y., Wada, E., Okada, M., Kanamatsu, T., & Taira, A. (1999). Sulfur isotope records around Livello Bonarelli (northern Apennines, Italy) black shale at the Cenomanian-Turonian boundary. *Geology*, *27*, 535–538. https://doi.org/10.1130/0091-7613(1999)027<0535:siralb>2.3.co;2

Owens, J. D., Gill, B. C., Jenkyns, H. C., Bates, S. M., Severmann, S., Kuypers, M. M. M., et al. (2013). Sulfur isotopes track the global extent and dynamics of euxinia during Cretaceous Oceanic Anoxic Event 2. *Proceedings of the National Academy of Sciences*, *110*(46), 18407–18412. https://doi.org/10.1073/pnas.1305304110

Pankina, R. G., Maksimov, S. P., Kalinko, M. K., Monakhov, I. B., & Guriyeva, S. M. (1975). Sulfur isotopic composition in the Phanerozoic evaporites of Bulgaria. *Geochemistry International*, *12*(6), 79–83.

Paytan, A., Kastner, M., Campbell, D., & Thiemens, M. H. (1998). Sulfur Isotopic Composition of Cenozoic Seawater Sulfate. *Science*, *282*, 1459–1462. https://doi.org/10.1126/science.282.5393.1459

Paytan, A., Kastner, M., Campbell, D., & Thiemens, M. H. (2004). Seawater Sulfur Isotope Fluctuations in the Cretaceous. *Science*, *304*, 1663–1665. https://doi.org/10.1126/science.1095258

Peryt, T. M., Halas, S., & Hryniv, S. P. (2010). Sulphur and oxygen isotope signatures of late Permian Zechstein anhydrites, West Poland: seawater evolution and diagenetic constraints. *Geological Quarterly*, *54*, 387–400.

Pisarchik, Y. K., & Golubchina, M. N. (1975). On isotope ratios of sulfur in the Cambrian sulfatic limestones of the Siberian platform. *Geochemistry International*, *12*, 227–230.

Playà, E., Cendón, D. I., Travé, A., Chivas, A. R., & García, A. (2007). Non-marine evaporites with both inherited marine and continental signatures: The Gulf of Carpentaria, Australia, at ~70 ka. *Sedimentary Geology*, *201*(3–4), 267–285. https://doi.org/10.1016/j.sedgeo.2007.05.010

Posey, H. H., & Fisher, S. R. (1989). A sulfur and strontium isotopic investigation of Lower Permian anhydrite, Palo Duro Basin, Texas, U.S.A. *Applied Geochemistry*, *4*(4), 395–407. https://doi.org/10.1016/0883-2927(89)90015-2

Poulton, S. W., Henkel, S., März, C., Urquhart, H., Flögel, S., Kasten, S., et al. (2015). A continental-weathering control on orbitally driven redox-nutrient cycling during Cretaceous Oceanic Anoxic Event 2. *Geology*, *43*(11), 963–966. https://doi.org/10.1130/G36837.1

Present, T. M. (2018). *Controls on the Sulfur Isotopic Composition of Carbonate-Associated Sulfate* (Ph.D.). California Institute of Technology, Pasadena, California. Retrieved from http://resolver.caltech.edu/CaltechTHESIS:04042018-153105432

Present, T. M., Paris, G., Burke, A., Fischer, W. W., & Adkins, J. F. (2015). Large Carbonate Associated Sulfate isotopic variability between brachiopods, micrite, and other sedimentary components in Late Ordovician strata. *Earth and Planetary Science Letters*, *432*, 187–198. https://doi.org/10.1016/j.epsl.2015.10.005

Present, T. M., Gutierrez, M., Paris, G., Kerans, C., Grotzinger, J. P., & Adkins, J. F. (2019). Diagenetic controls on the isotopic composition of carbonate-associated sulphate in the Permian Capitan Reef Complex, West Texas. *Sedimentology*, *66*(7), 2605–2626. https://doi.org/10.1111/sed.12615

Prokoph, A., Shields, G. A., & Veizer, J. (2008). Compilation and time-series analysis of a marine carbonate δ18O, δ13C, 87Sr/86Sr and δ34S database through Earth history. *Earth-Science Reviews*, *87*(3–4), 113–133. https://doi.org/10.1016/j.earscirev.2007.12.003

Qiu, Z., Sun, S., Wei, H., Wang, Q., Zou, C., & Zhang, Y. (2015). SIMS zircon U-Pb dating from bentonites in the Penglaitan Global Stratotype Section for the Guadalupian–Lopingian boundary (GLB), South China. *Geological Journal*.

Rennie, V. C. F., & Turchyn, A. V. (2014). The preservation of d34SSO4 and d18OSO4 in carbonate-associated sulfate during marine diagenesis: A 25 Myr test case using marine sediments. *Earth and Planetary Science Letters*, *395*, 13–23. https://doi.org/10.1016/j.epsl.2014.03.025

Rennie, V. C. F., Paris, G., Sessions, A. L., Abramovich, S., Turchyn, A. V., & Adkins, J. F. (2018). Cenozoic record of δ 34 S in foraminiferal calcite implies an early Eocene shift to deep-ocean sulfide burial. *Nature Geoscience*, (11), 761–765. https://doi.org/10.1038/s41561-018-0200-y

Riccardi, A. L., Arthur, M. A., & Kump, L. R. (2006). Sulfur isotopic evidence for chemocline upward excursions during the end-Permian mass extinction. *Geochimica et Cosmochimica Acta*, *70*, 5740–5752.

Richardson, J. A., Keating, C., Lepland, A., Hints, O., Bradley, A. S., & Fike, D. A. (2019). Silurian records of carbon and sulfur cycling from Estonia: The importance of depositional environment on isotopic trends. *Earth and Planetary Science Letters*, *512*, 71–82. https://doi.org/10.1016/j.epsl.2019.01.055

Rine, M. J., Garrett, J. D., & Kaczmarek, S. E. (2017). A New Facies Architecture Model for the Silurian Niagaran Pinnacle Reef Complexes of the Michigan Basin. In A. J. Macneil, J. Lonnee, & R. Wood, *Characterization and Modeling of Carbonates–Mountjoy Symposium 1*. SEPM (Society for Sedimentary Geology). https://doi.org/10.2110/sepmsp.109.02

Rose, C. V., Fischer, W. W., Finnegan, S., & Fike, D. A. (2019). Records of carbon and sulfur cycling during the Silurian Ireviken Event in Gotland, Sweden. *Geochimica et Cosmochimica Acta*, *246*, 299–316. https://doi.org/10.1016/j.gca.2018.11.030

Sakai, H. (1972). Oxygen isotopic ratios of some evaporites from Precambrian to Recent ages. *Earth and Planetary Science Letters*, *15*(2), 201–205. https://doi.org/10.1016/0012-821X(72)90061-1

Saltzman, M. R., Cowan, C. A., Runkel, A. C., Runnegar, B., Stewart, M. C., & Palmer, A. R. (2004). The Late Cambrian Spice (δ13C) Event and the Sauk II-SAUK III Regression: New Evidence from Laurentian Basins in Utah, Iowa, and Newfoundland. *Journal of Sedimentary Research*, *74*(3), 366–377. https://doi.org/10.1306/120203740366

Schobben, M., Stebbins, A., Ghaderi, A., Strauss, H., Korn, D., & Korte, C. (2015). Flourishing ocean drives the end-Permian marine mass extinction. *Proceedings of the National Academy of Sciences*, *112*(33), 10298–10303. https://doi.org/10.1073/pnas.1503755112

Schobben, M., Stebbins, A., Algeo, T. J., Strauss, H., Leda, L., Haas, J., et al. (2017). Volatile earliest Triassic sulfur cycle: A consequence of persistent low seawater sulfate concentrations and a high sulfur cycle turnover rate? *Palaeogeography, Palaeoclimatology, Palaeoecology*, *486*, 74–85. https://doi.org/10.1016/j.palaeo.2017.02.025

Schrag, D. P., DePaolo, D. J., & Richter, F. M. (1995). Reconstructing past sea surface temperatures: Correcting for diagenesis of bulk marine carbonate. *Geochimica et Cosmochimica Acta*, *59*(11), 2265–2278. https://doi.org/10.1016/0016-7037(95)00105-9

Schröder, S., Schreiber, B. C., Amthor, J. E., & Matter, A. (2004). Stratigraphy and environmental conditions of the terminal Neoproterozoic–Cambrian Period in Oman: evidence from sulphur isotopes. *Journal of the Geological Society*, *161*(3), 489–499. https://doi.org/10.1144/0016-764902-062

Sim, M. S., Ono, S., & Hurtgen, M. T. (2015). Sulfur isotope evidence for low and fluctuating sulfate levels in the Late Devonian ocean and the potential link with the mass extinction event. *Earth and Planetary Science Letters*, *419*, 52–62. https://doi.org/10.1016/j.epsl.2015.03.009

Solomon, M., Rafter, T. A., & Dunham, K. C. (1971). Sulphur and oxygen isotope studies in the northern Pennines in relation to ore genesis. *Transactions of the Institution of Mining and Metallurgy Section B*, *80B*, 259–275.

Song, H., Tong, J., Algeo, T. J., Song, H., Qiu, H., Zhu, Y., et al. (2014). Early Triassic seawater sulfate drawdown. *Geochimica et Cosmochimica Acta*, *128*(0), 95–113. https://doi.org/10.1016/j.gca.2013.12.009

Song, H., Du, Y., Algeo, T. J., Tong, J., Owens, J. D., Song, H., et al. (2019). Cooling-driven oceanic anoxia across the Smithian/Spathian boundary (mid-Early Triassic). *Earth-Science Reviews*. https://doi.org/10.1016/j.earscirev.2019.01.009

Spötl, C. (1988). Schwefelisotopendatierungen und fazielle Entwicklung permoskytischer Anhydrite in den Salzbergbauen von Dürrnberg/Hallstein und Hallstadt (Österreich). *Mitteilungen Der Gesellschaft Der Geologie- Und Bergbaustudenten in Österreich*, *34–35*, 209–229.

Stebbins, A., Algeo, T. J., Krystyn, L., Rowe, H., Brookfield, M., Williams, J., et al. (2019). Marine sulfur cycle evidence for upwelling and eutrophic stresses during Early Triassic cooling events. *Earth-Science Reviews*. https://doi.org/10.1016/j.earscirev.2018.09.007

Stollhofen, H., Bachmann, G. H., Barnasch, J., Bayer, U., Beutler, G., Franz, M., et al. (2008). Upper Rotliegend to early cretaceous basin development. *Dynamics of Complex Intracontinental Basins. The Central European Basin System*, 181–210.

Taki, H. E., & Pratt, B. R. (2012). Syndepositional tectonic activity in an epicontinental basin revealed by deformation of subaqueous carbonate laminites and evaporites: Seismites in Red River strata (Upper Ordovician) of southern Saskatchewan, Canada. *Bulletin of Canadian Petroleum Geology*, *60*(1), 37–58. https://doi.org/10.2113/gscpgbull.60.1.37

Thode, H. G., & Monster, J. (1965). Sulfur-Isotope Geochemistry of Petroleum, Evaporites, and Ancient Seas. In A. Young & J. E. Galley (Eds.), *AAPG Memoir 4: Fluids in subsurface environments* (Vol. 71, pp. 367–377). Tulsa, Oklahoma: American Association of Petroleum Geologists. Retrieved from http://archives.datapages.com/data/specpubs/methodo2/data/a071/a071/0001/0350/0367.htm

Thode, H. G., & Monster, J. (1970). Sulfur Isotope Abundances and Genetic Relations of Oil Accumulations in Middle East Basin. *AAPG Bulletin*, *54*(4), 627–637.

Thode, H. G., Monster, J., & Dunford, H. B. (1958). Sulphur Isotope Abundances in Petroleum and Associated Materials. *AAPG Bulletin*, *42*(11), 2619–2641.

Thompson, Cara K., & Kah, L. C. (2012). Sulfur isotope evidence for widespread euxinia and a fluctuating oxycline in Early to Middle Ordovician greenhouse oceans. *Palaeogeography, Palaeoclimatology, Palaeoecology*, *313–314*(0), 189–214. https://doi.org/10.1016/j.palaeo.2011.10.020

Thompson, Cara K., Kah, L. C., Astini, R., Bowring, S. A., & Buchwaldt, R. (2012). Bentonite geochronology, marine geochemistry, and the Great Ordovician Biodiversification Event (GOBE). *Palaeogeography, Palaeoclimatology, Palaeoecology*, *321–322*(0), 88–101. https://doi.org/10.1016/j.palaeo.2012.01.022

Thompson, Cara Kim. (2011). *Carbon and Sulfur Cycling in Early Paleozoic Oceans* (Ph.D. diss). University of Tennessee, Knoxville.

Turchyn, A. V., Schrag, D. P., Coccioni, R., & Montanari, A. (2009). Stable isotope analysis of the Cretaceous sulfur cycle. *Earth and Planetary Science Letters*, *285*, 115–123. https://doi.org/10.1016/j.epsl.2009.06.002

Utrilla, R., Pierre, C., Orti, F., & Pueyo, J. J. (1992). Oxygen and sulphur isotope compositions as indicators of the origin of Mesozoic and Cenozoic evaporites from Spain. *Chemical Geology*, *102*(1), 229–244. https://doi.org/10.1016/0009-2541(92)90158-2

Vinogradov, V. I. (2007). Was there a conflict at the Neoproterozoic-Cambrian boundary: Evidence from sulfur isotope composition? *Lithology and Mineral Resources*, *42*(1), 1–14. https://doi.org/10.1134/S0024490207010014

Voigt, S., Erbacher, J., Mutterlose, J., Weiss, W., Westerhold, T., Wiese, F., et al. (2008). The Cenomanian – Turonian of the Wunstorf section – (North Germany): global stratigraphic reference section and new orbital time scale for Oceanic Anoxic Event 2. *Newsletters on Stratigraphy*, *43*(1), 65–89. https://doi.org/10.1127/0078-0421/2008/0043-0065

Vredenburgh, L. D., & Cheney, E. S. (1971). Sulfur and carbon isotopic investigation of petroleum, Wind River basin, Wyoming. *AAPG Bulletin*, *55*(11), 1954–1975.

Webster, R., & Oliver, M. A. (2007). *Geostatistics for environmental scientists* (2nd ed.). Chichester, UK: Wiley.

Wei, W., & Gartner, S. (1993). 2. Neogene Calcareous Nannofossils from Sites 811 and 819 Through 825, offshore Northeastern Australia. In J. A. McKenzie, P. J. Davies, & A. Palmer-Julson (Eds.), *Scientific Results* (Vol. 133, pp. 19–37). College Station, Texas: Ocean Drilling Program. https://doi.org/10.2973/odp.proc.sr.133.1993

Westerhold, T., Röhl, U., Raffi, I., Fornaciari, E., Monechi, S., Reale, V., et al. (2008). Astronomical calibration of the Paleocene time. *Palaeogeography, Palaeoclimatology, Palaeoecology*, *257*(4), 377–403. https://doi.org/10.1016/j.palaeo.2007.09.016

Witts, J. D., Newton, R. J., Mills, B. J. W., Wignall, P. B., Bottrell, S. H., Hall, J. L. O., et al. (2018). The impact of the Cretaceous–Paleogene (K–Pg) mass extinction event on the global sulfur cycle: Evidence from Seymour Island, Antarctica. *Geochimica et Cosmochimica Acta*. https://doi.org/10.1016/j.gca.2018.02.037

Worden, R. H., Smalley, P. C., & Fallick, A. E. (1997). Sulfur cycle in buried evaporites. *Geology*, *25*(7), 643–646. https://doi.org/10.1130/0091-7613(1997)025<0643:SCIBE>2.3.CO;2

Wotte, T., Strauss, H., & Sundberg, F. A. (2011). Carbon and Sulfur Isotopes from the Cambrian Series 2-Cambrian Series 3 of Laurentia and Siberia. In J. S. Hollingsworth, F. A. Sundberg, & J. R. Foster (Eds.), *Museum of Northern Arizona Bulletin 67: Cambrian Stratigraphy and Paleontology of Northern Arizona and Southern Nevada: The 16th Field Conference of the Cambrian Stage Subdivision Working Group, International Subcommission on Cambrian Stratigraphy, Flagstaff, Arizona, and Southern Nevada, United States* (pp. 43–63). Flagstaff, Arizona: Museum of Northern Arizona.

Wotte, T., Shields-Zhou, G. A., & Strauss, H. (2012). Carbonate-associated sulfate: Experimental comparisons of common extraction methods and recommendations toward a standard analytical protocol. *Chemical Geology*, *326–327*, 132–144. https://doi.org/10.1016/j.chemgeo.2012.07.020

Wright, J. D., & Kroon, D. (2000). Planktonic foraminiferal biostratigraphy of Leg 166. In P. K. Swart, G. P. Eberli, M. J. Malone, & J. F. Sarg (Eds.), *Scientific Results* (Vol. 166, pp. 3–12). College Station, Texas: Ocean Drilling Program. https://doi.org/10.2973/odp.proc.sr.166.2000

Wu, N. (2013). *Sulfur isotopic evolution of Phanerozoic and Ediacaran seawater sulfate*. University of Maryland, College Park, Md. Retrieved from http://hdl.handle.net/1903/14016

Wu, N., Farquhar, J., & Strauss, H. (2014). δ34S and Δ33S records of Paleozoic seawater sulfate based on the analysis of carbonate associated sulfate. *Earth and Planetary Science Letters*, *399*(0), 44–51. https://doi.org/10.1016/j.epsl.2014.05.004

Wu, Q., Ramezani, J., Zhang, H., Yuan, D., Erwin, D. H., Henderson, C. M., et al. (2020). High-precision U-Pb zircon age constraints on the Guadalupian in West Texas, USA. *Palaeogeography, Palaeoclimatology, Palaeoecology*, *548*, 109668. https://doi.org/10.1016/j.palaeo.2020.109668

Yadong, S., Xulong, L., Haishui, J., Genming, L., Si, S., Chunbo, Y., & Wignall, P. B. (2008). Guadalupian (Middle Permian) Conodont Faunas at Shangsi Section, Northeast Sichuan Province. *Journal of China University of Geosciences*, *19*(5), 451–460. https://doi.org/10.1016/S1002-0705(08)60050-3

Yan, D., Zhang, L., & Qiu, Z. (2013). Carbon and sulfur isotopic fluctuations associated with the end-Guadalupian mass extinction in South China. *Gondwana Research*, *24*(3–4), 1276–1282. https://doi.org/10.1016/j.gr.2013.02.008

Yang, C., Li, X.-H., Zhu, M., Condon, D. J., & Chen, J. (2018). Geochronological constraint on the Cambrian Chengjiang biota, South China. *Journal of the Geological Society*, *175*(4), 659–666. https://doi.org/10.1144/jgs2017-103

Yao, W., Paytan, A., & Wortmann, U. G. (2018). Large-scale ocean deoxygenation during the Paleocene-Eocene Thermal Maximum. *Science*, *361*(6404), 804–806. https://doi.org/10.1126/science.aar8658

Yao, W., Paytan, A., Griffith, E. M., Martínez-Ruiz, F., Markovic, S., & Wortmann, U. G. (2020). A revised seawater sulfate S-isotope curve for the Eocene. *Chemical Geology*, *532*, 119382. https://doi.org/10.1016/j.chemgeo.2019.119382

Yeremenko, N. A., & Pankina, R. G. (1972). Variations of 34S in Sulfates of Recent and Ancient Marine Basins of the Soviet Union. *Geochemistry International*, *10*, 45–54.

Young, S. A., Gill, B. C., Edwards, C. T., Saltzman, M. R., & Leslie, S. A. (2016). Middle–Late Ordovician (Darriwilian–Sandbian) decoupling of global sulfur and carbon cycles: Isotopic evidence from eastern and southern Laurentia. *Palaeogeography, Palaeoclimatology, Palaeoecology*, *458*, 118–132. https://doi.org/10.1016/j.palaeo.2015.09.040

Young, S. A., Kleinberg, A., & Owens, J. D. (2019). Geochemical evidence for expansion of marine euxinia during an early Silurian (Llandovery–Wenlock boundary) mass extinction. *Earth and Planetary Science Letters*, *513*, 187–196. https://doi.org/10.1016/j.epsl.2019.02.023

Zhang, L., Zhao, L., Chen, Z.-Q., Algeo, T. J., Li, Y., & Cao, L. (2015). Amelioration of marine environments at the Smithian–Spathian boundary, Early Triassic. *Biogeosciences*, *12*(5), 1597–1613.

Zhu, M., Yang, A., Yuan, J., Li, G., Zhang, J., Zhao, F., et al. (2019). Cambrian integrative stratigraphy and timescale of China. *Science China Earth Sciences*, *62*(1), 25–60. https://doi.org/10.1007/s11430-017-9291-0